Ernest H. H. Shih
Department of Geosciences and Office of Arid Lands Studies
University of Arizona
Tucson, AZ 85719
Robert A. Schowengerdt
Office of Arid Lands Studies and Electrical Engineering Department
University of Arizona
Tucson, AZ 85719

Classification of Arid Geomorphic Surfaces Using Landsat Spectral and Textural Features

The addition of image texture improves class separability by incorporating geomorphic terrain parameters

Abstract: *A computationally efficient texture extraction algorithm which measures the local edge amplitude and density of an image is used to derive textural features from Landsat MSS data. Three of these derived textural features are added to the original four Landsat bands in a multifeature geomorphic classification of a natural arid terrain. The addition of textural features significantly improved training class separability when compared to a spectral only classification. Classification improvement, as determined by photointerpretation and by comparison to a geologic/geomorphic map, was significant. Discrimination between classes which have large spectral overlap but are texturally distinct, such as darkly varnished bedrock slopes and desert pavement surfaces, and lightly colored bedrock and alluvial surfaces, was the area of greatest improvement.*

Introduction

In traditional geologic and geomorphic mapping, interpretation from aerial photography and field reconnaissance are the main sources of information. When mapping geomorphologic features, the geologist must first determine mapping units on the basis of detailed field examination involving stratigraphy and soil analysis. After the initial classes are defined, the geologist generally maps, both in the field and from air photos, on the basis of parameters such as surface topography, color, tone, morphology, drainage pattern, and vegetation.

On multispectral satellite imagery, such as that from the Landsat Multispectral Scanner (MSS), these parameters often contribute heterogeneity, rather than homogeneity, to geomorphic class signatures. For example, many geomorphic classes appear as a repetitive spatial pattern of tonal (grey-level) variation (texture) whose characteristics are controlled by one or more of these parameters. The result is a large variance in class grey-level distribution. Compounding the problem of tonal variation within geomorphic classes is the existence of weathered surfaces or surface coatings in many natural environments. These tend to reduce spectral differences between geomorphically distinct classes. Consequently, the experienced geomorphologist uses textural analysis in support of tonal analysis as a key photoanalytic tool for the differentiation of geomorphic classes.

In computer-assisted mapping from such imagery, classifications based only on spectral features are usually insufficient for high-level differentiation of geomorphic surfaces. Our objective was to

Photogrammetric Engineering and Remote Sensing,
Vol. 49, No. 3, March 1983, pp. 337-347.

0099-1112/83/4903-0337$02.25/0
© 1983 American Society of Photogrammetry

develop an improved methodology for the production of geomorphic maps using both spectral and textural features as data sources for digital image classification.

Desert Varnish and Desert Pavement

In arid terrain, the darkness of a rock surface coating called *desert varnish* creates much of the spectral ambiguity between bedrock and desert pavement surfaces. Desert varnish is a dark amorphous coating of clays and ferromanganese oxides which is found with near ubiquity on any relatively stable surface in the desert. The chemistry and structure of desert varnish has been studied in depth (Engel and Sharp, 1958; Hunt, 1961; Hooke *et al.*, 1969; Potter and Rossman, 1977; Perry and Adams, 1978). However, the exact mechanism involved in the formation of desert varnish is still not well understood. It is generally agreed that both clays and oxides are from eolian deposition. Potter and Rossman (1977) have argued that the clay may act as a manganese fixing agent whereas others (Scheffer *et al.*, 1963; Bauman, 1976; Perry and Adams, 1978; Dorn, 1980) have argued that it is a product of biological activity by microorganisms.

One of the darkest geomorphic surfaces in the desert is that called desert pavement. Desert pavement, also called stone pavement or hamada, is a stony surface mantle that, when fully developed, forms a dark planar surface of size-sorted stones so well fitted together that the surface has the appearance of a rock mosaic or pavement. Desert pavements have been found and described in most of the arid regions of the world (Blake, 1904; Sharon, 1962; Springer, 1958; Symmons and Hemming, 1968; Cooke, 1970). Three mechanisms have been suggested for the formation of desert pavement: water sorting, wind deflation, and upward migration of stones. Cooke and Warren (1973) have reviewed much of the literature on this subject.

The darkness of desert varnish on both bedrock and desert pavement surfaces is a function of the physical weathering attributes of the rock material, the relative age of that surface, and its particle size distribution (Shih, 1982). Rocks that are lithologically similar may have dramatically different weathering characteristics and therefore have quite different surface spectral signatures. On the other hand, rocks that are dissimilar in lithology may have similar weathering characteristics and similar varnish coatings. These lithologic classes are impossible to separate by spectral signature alone but could in some cases be separated by image textural attributes.

Image Texture

In digital imagery, *texture* can be defined as patterns of spatial relationships, often quite complex, among the grey levels of neighboring pixels. The importance of image texture in geologic terrain classification has been demonstrated in experiments by Haralick *et al.* (1973) and by Weszka *et al.* (1976). Weszka *et al.* (1976) were able to distinguish three rock types from 180 samples with accuracies of up to 95 percent based on textural measures alone.

Although textural features have been increasingly incorporated into multispectral classification (Wiersma and Landgrebe, 1976; Hsu, 1978; Jensen, 1979; Fasler, 1980; Irons and Petersen, 1981; Jensen and Toll, 1982), no single algorithm combining both efficiency and effectiveness has been widely accepted. Numerous textural measures have been developed. Literature surveys and algorithm comparisons are given in Weszka, *et al.* (1976), Haralick (1979), and Conners and Harlow (1980).

Hsu (1979) divided textural measures into two broad categories: Fourier-based features and statistical features. Weszka *et al.* (1976) demonstrated the superiority of statistical features over Fourier-based features. The most commonly used set of statistical features are the second-order textural measures based on Haralick's grey-tone spatial dependency matrix (Haralick, 1979). However, these textural measures incur large computational cost when used on a pixel-by-pixel basis. Mitchell's max-min textural measures has been shown to perform equally well or slightly better but with less computational effort (Mitchell *et al.*, 1977).

The max-min method uses the relative number of local grey-level extrema as the principal textural measure. In the one-dimensional case, a pixel is classified as a local extremum if it is the largest (or smallest) value before the values drop (or rise) to a value T (Carlton and Mitchell, 1977).

Local extrema may be divided into specific threshold ranges, each defined by a different value T. In the case of three thresholds (T_1, T_2, T_3), an individual pixel is classified as either not an extremum or an extremum of threshold T_1, T_2, or T_3. The texture at any given pixel is defined by the number of pixels within each threshold range within a given neighborhood.

Our goal was to devise a relatively simple and efficient texture feature extraction algorithm similar to Mitchell's max-min measure that could be easily implemented with common image processing software.

Study Area

The study area is a 296 square kilometre (110 square mile) site in the extremely arid Kofa Game Range of southwestern Arizona (Figure 1). The site, typical of basin and range topography (Fenneman, 1931), includes portions of the Castle Dome Mountains, its alluvium mantled pediment, and portions of King Valley to the east of the range.

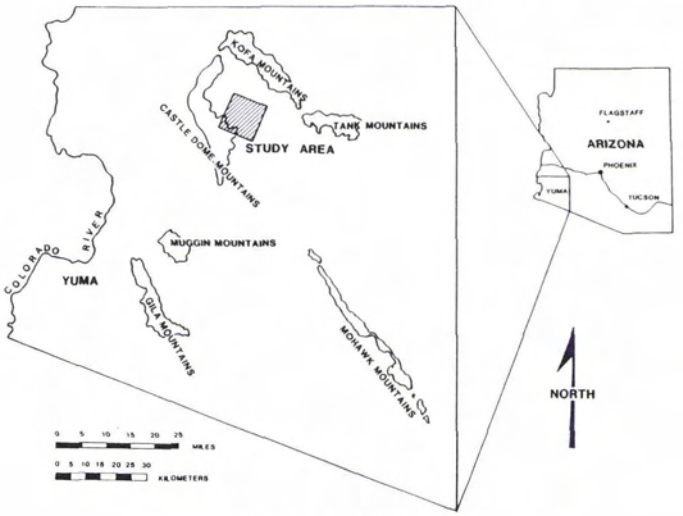

FIG. 1. Location of study site.

GEOLOGY AND GEOMORPHOLOGY

A generalized geologic/geomorphic sketch map of the study area (Figure 2) was interpreted from field data and 1:24,000-scale aerial photography. The Landsat band 5 image of the same area, extracted from scene E-1194-17391, 2 February 1973, is shown in Figure 3. The site can be divided into three major regions. From southwest to northeast these are mountain range, alluvium-mantled pediment plain, and the axial stream complex of the basin.

Within the study area, the mountain range is composed primarily of Tertiary volcanic rocks but also contains two large areas of Mesozoic sedimentary and metamorphic rocks. In a standard Landsat false color composite, the Mesozoic rocks are spectrally distinguished from other rocks by their blue color. Within the mountain range are patches of elevated Q2a and Q2b geomorphic surfaces, which are formed on a now dissected Middle Pleistocene fan (Table 1). Geomorphic terms and classification systems used in our tables and maps were adapted from a manuscript by Bull (in preparation). In the Landsat image, the low reflectance caused by desert varnish coatings on most of the volcanic rocks (Tvf, Ta, Trt) and desert pavement surfaces (Q2a, Q2b, Q2c) makes it difficult to distinguish these classes by spectral reflectance alone.

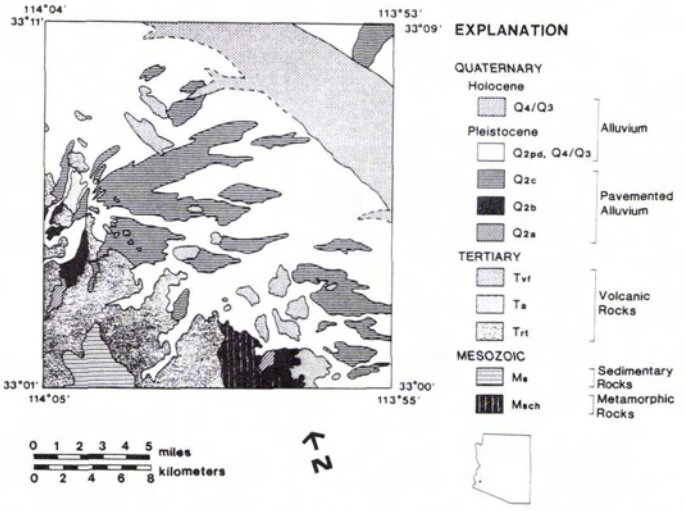

FIG. 2. Geologic/geomorphic sketch map. (Refer to Table 1 for description of geologic units.)

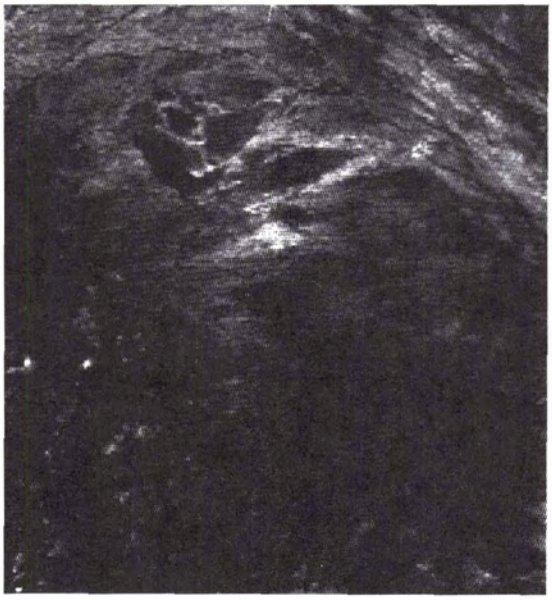

FIG. 3. Landsat Band 5 extracted image.

TABLE 1. GEOLOGIC/GEOMORPHIC CLASSES OF SKETCH MAP

Class	Description
Q4/Q3	Modern alluvium, stream channels, flood plains, overbank deposits.
Q2pd, Q4/Q3	Complex of Pleistocene and Modern alluvium: stable and partially or fully degraded or dissected pavement.
Q2c	Late Pleistocene alluvium. Flat, stable desert pavement.
Q2b	Middle Pleistocene alluvium. Moderately dissected desert pavement, ridge, and ravine topography.
Q2a	Middle Pleistocene alluvium, highly dissected, with remnants of desert pavement. Hill and valley topography.
Tvf	Acid to Acid-intermediate volcanic flows and pyroclastics.
Ta	Basaltic andesites.
Trt	Rhyolitic ash-flow tuffs and banded rhyolites, faulted and tilted.
Ms	Sedimentary and low-grade metamorphic rocks of sedimentary origin (slates, limestones, conglomerates, sandstones, and quartzites).
Msch	Mesozoic schists.

The alluvium-mantled pediment plain, the second region, is composed of inselbergs (bedrock outliers surrounded by alluvium), alluvial surfaces, and ephemeral washes. Late Pleistocene dark pavement surfaces (Q2c) are quite widespread, although Holocene fluvial activity has reduced the once continuous fan of dark stable desert pavement into a complex of interdigitated stable desert pavements (Q2c), vertically degraded desert pavements (Q2pd), and modern erosional surfaces (Q4/Q3). Degraded pavements are those surfaces which are recognized as vertically eroded desert pavements by diagnostic horizons in their truncated soils and by stratigraphic considerations. Modern erosional surfaces have no evidence of soil development and show signs of recent fluvial erosion. Ephemeral washes are recognized by channel type deposits and by their associated riparian vegetation.

Desert varnish makes both bedrock inselbergs and desert alluvial pavements dark. These classes are differentiated on satellite images by the shadowed and illuminated slope textures associated with inselbergs and a grainy mottled texture associated with dark desert pavements. Dissected desert pavements have a grainy mottling texture along with numerous fine filaments created by dissection channels. Degraded pavements have an even light tone whereas erosional surfaces are recognized by uneven light tones.

The axial stream complex, the third region, is composed of anastomosing sand and gravel channels and dense riparian vegetation. Between the channels are flat overbank deposits of sand and silt, often covered with creosote bush (*Larrea divaricata*). The entire region is generalized in the sketch map as Q4/Q3.

TEXTURE FEATURE EXTRACTION

An algorithm that measures local edge amplitude and density (LEAD) was developed and used to extract texture features from the Landsat data. This texture algorithm is similar to the local max-min extrema measure described by Mitchell *et al.* (1977) and by Carlton and Mitchell (1977). The main difference between our algorithm and that of Mitchell *et al.* is that ours measures all local pixel deviations within a specified threshold range and does not look for local extrema only. The ease of computation, efficiency, and reported success of local extrema textural measures (max-min) (Mitchell *et al.*, 1977) were the reasons for using this approach.

METHOD

Texture feature extraction by the LEAD method was done in three steps (Figure 4). The first step was the convolution of the band 5 Landsat image with a 3-by-3 high pass spatial filter. As illustrated in Figure 4, Step 1, this produced a high pass image with an approximately normal grey-level distribution about a mean of zero. High pass filtering removes low frequency background variations and only allows the high frequency image information to remain. The rationale for using a high pass filter follows from the intuition that tex-

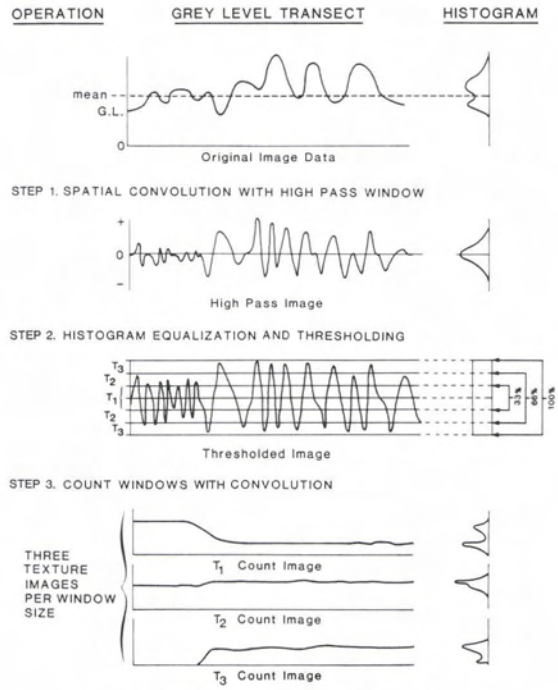

FIG. 4. Texture feature extraction.

tural information is primarily found in local contrast variations; that is, the human eye recognizes similar textures regardless of average background grey level. Sharp transitions in radiance levels (edges) in the original image become spikes in the high pass image, with the sharpness and amplitude of the spikes dependent on the width and contrast of the transitions in the original image.

In the second step (Figure 4, Step 2), two absolute value thresholds were applied to the high pass image so that each pixel was classified into one of three mutually exclusive threshold ranges. These threshold ranges are analogous to the T_1, T_2, T_3 grey-level distances of Carlton and Mitchell (1977). Because no *a priori* arguments exist for the placement of threshold boundaries, it was decided that these thresholds would be set by an equal probability rule that could be implemented automatically. The procedure was simply to perform a contrast stretch which equalized the grey-level probabilites (histogram equalization) in the high pass image. Thresholds were chosen at points that divided the resulting uniform histogram into three equal areas.

In step three (Figure 4, Step 3), a count image was produced by convolving the thresholded high pass image with a window that counts the number of pixels in each threshold range within the window area. The number of pixels within each range is a measure of a specific amplitude (T_1, T_2, and T_3 range limits) and density (number of points within each range) of image *activity;* that is, edges, lines, points, and other elements of texture within the neighborhood defined by the window.

Our choice of window sizes was guided by empirical information. Window sizes of 5-by-5, 9-by-9, and 11-by-11 pixels were used because we had observed from the Landsat image that the most significant textural variations were of this scale. For example, the texture of shadowed and illuminated slopes of bedrock has a spatial frequency of one cycle per 5 to 11 pixels, with a cycle consisting of one shadowed and one illuminated slope. The texture of a moderately dissected desert pavement, consisting of dark grainy flat areas with fine filaments and mottles, has several cycles per 5 to 11 pixels. Each combination of window size and threshold range produced one textural feature. Three window sizes and three thresholds were used, so that a total of nine features were derived from the original Landsat band 5 data.

Classification and Feature Selection

All classifications were performed using a supervised classification program employing the Bayesian maximum-likelihood rule. Twelve *spectral/geomorphic* classes (Table 2) were defined on the basis of extensive field investigation and interpretation of Landsat images and aerial photos (Shih, 1982). Their defining characteristics are based on reflectance data as well as geomorphic data. Bedrock classes, which are differentiated lithologically in the geologic/geomorphic system, are grouped by reflectance in the spectral/geomorphic classes. Alluvial classes are more refined in the spectral/geomorphic system. They are classified on the basis of reflectance, age, and relative erosional activity or stability of the surfaces. The complex of surfaces in the pediment and basin regions, regions 2 and 3, which are generalized in the sketch map, is divided into two pavement classes, two erosional classes, and three vegetation and (active) fluvial classes.

Twenty-five training sites were selected to represent these spectral/geomorphic classes. Because of the limited spatial extent of many of the classes, some of the training sites were by necessity very small. However, all training classes were defined by at least nine samples (per feature). The larger sites usually consisted of 25 samples, with the largest having 64 samples. The final pixel coordinates of all sites were located interactively on a video color display.

Training site statistics were generated for all nine textural features. The between-class divergence (Swain and Davis, 1978) was calculated for all pairs of classes and textural feature combinations. This was used as a criterion to reduce the number of features to only the most useful ones. The combination of three features that produced

TABLE 2. SPECTRAL/GEOMORPHIC CLASS DESCRIPTIONS USED IN LANDSAT CLASSIFICATION

No.	Name	Description	Equivalent Geologic-Geomorphic Classes
		Bedrock	
1	ROCKL	Rock hills and hillslopes with no desert varnish—light-colored irregularly weathered surface. Mostly tuffs and flow-banded rhyolites.	Trt
2	ROCKD	Dark rock hills and hillslopes, with composition ranging from rhyolitic to basaltic andesitic volcanic rocks—all heavily coated with desert varnish.	Trt, Ta, Tvf
3	ROCKB	Rock hills, hillslopes, and associated alluvium of Mesozoic sedimentary and metamorphic rock, generally weathered to a grey green color and having a blue color in the Landsat standard false-color composite images.	Ms, Msch
4	Q2a	Highly dissected alluvial surface of early Middle Pleistocene age. Limited in extent, rounded hill and valley morphology (forming smooth concave and convex surfaces), a few remnant dark desert pavement surfaces, and exposed caliche clasts.	Q2a
5	Q2b	Dissected alluvial surface of Middle Pleistocene age; flat top ridges and concave valley morphology. Dark desert pavements on ridge.	Q2b
6	Q2*cd*	Darkest desert pavement of Late Pleistocene age, very flat with darkly varnished rock armor; moderate dissection. Darker due to enhanced varnish on more basic volcanic rocks (quartz latite, basaltic andesite, etc.).	Q2c
7	Q2*cl*	Dark desert pavement of Late Pleistocene age but lighter than Class 6. Surface is flat, with limited dissection. Varnish dark but lighter than Q2*cd* in part due to more acidic rock composition.	Q2c
		Eroded Desert Pavement	
8	PAV DIS	Desert pavement vertically degraded by sheetwash erosion; a very flat planar surface which is light in color due to exposed sand, silts, and clays, with caliche clasts on surface. In areas, alternating with patches of Q2*cd*, Q2*cl*, and C EROS.	Q2pd, Q4/Q3
9	C EROS	Coarse erosional surface, a gravelly modern surface mostly composed of coarse unvarnished rocks of mixed lithology and reflectances, with no soil development and sparse vegetation; low relief and undulating surface morphology.	Q4/Q3
		Modern Fluvial Deposits and Vegetation	
10	SAND	Overbank deposits of fine sand and silt with varying amounts of creosote bush in pure stands.	Q4/Q3
11	WRP	Relatively unchannelized wide ephemeral floodway composed of sand and gravels with open clustered riparian vegetation.	Q4/Q3
12	DRP	Major incised ephemeral stream channels with dense riparian vegetation.	Q4/Q3

the highest average between-class divergence was found to be the high threshold 5-by-5 window size (T_H 5-by-5), high threshold 9-by-9 window size (T_H 9-by-9), and the low threshold 11-by-11 window size (T_L 11-by-11). These textural features were then merged with the four Landsat spectral bands. Of all seven features, the best combination of four features (highest average between-class divergence) was Landsat MSS bands 5 and 6, and textural features T_H 5-by-5 and T_L 11-by-11.

Three classification maps were made; the first from the four Landsat bands (spectral); the second from the best combination of four features, two spectral and two textural features (best four); and the third from all seven features, the four Landsat bands and the best set of three textural features (spectral plus textural). In all cases, "best" was defined as the combination of features that yielded the highest average between-class divergence. Training site statistics are shown for all three classifications in Table 3. The "best four" classification was intermediate in class separability to the other two and, overall, showed little improvement over the "spectral" classification because the in-

TABLE 3. PERFORMANCE BASED ON TRAINING SITE STATISTICS

Class (# Pixels)		Percent Correct		
		Spectral	Best Four	Spectral plus Textural
1 ROCKL	(9)	55.6	100.0	100.0
2 ROCKD	(100)	44.0	91.0	93.0
3 ROCKB	(25)	96.0	68.0	100.0
4 Q2A	(9)	88.9	100.0	100.0
5 Q2B	(9)	100.0	100.0	100.0
6 Q2*cd*	(31)	71.0	93.5	100.0
7 Q2*cl*	(50)	70.0	94.0	94.0
8 PAV DIS	(34)	73.5	79.4	94.1
9 C EROS	(34)	44.1	55.9	88.2
10 SAND	(95)	75.8	89.5	97.9
11 WRP	(9)	88.9	100.0	100.0
12 DRP	(19)	68.4	63.2	84.2
AVERAGE	35	73.0	86.2	96.0

clusion of two textural features was insufficient to compensate for the deletion of two spectral bands. Therefore, the remainder of the discussion in this paper will be related to the "spectral-only" and the seven-band "spectral plus textural" classifications.

RESULTS

Classification with the addition of textural features was better than expected considering the geomorphic complexity of the site and the fineness of the spectral-geomorphic class divisions (Table 2). The inclusion of textural features significantly improved overall classification accuracy *within the training sites*. Accuracies improved from an average of 73 percent in the "spectral" classification to 96 percent in the "spectral plus textural" classification (Table 3). Improvements were especially significant in the separation of class 2, dark bedrock, from the desert pavement classes 4, 5, 6, and 7 (Figure 5).

As illustrated in the grey-level plots (Figure 5), textural, not spectral, features separate the dark bedrock class, 2, from pavement classes 4, 5, 6, and 7. Because class 2 is composed of hillslopes, the radiance range of this class is large in each of the Landsat bands, as illustrated by the grey-level standard deviation of spectral bands. But textural features separate class 2 from the pavement classes because of its larger number of high threshold pixels (T_H 5-by-5, T_H 9-by-9) and smaller number of low threshold pixels (T_L 11-by-11). Two of the textural features also separate classes 5 and 6, which are not separable in the original spectral bands (Figure 5). Class 5 (Q2b) has dark pavement but is characterized by greater relief than class 6 (Q2*cd*), which is equally dark. Because of this relief, textural features produced with larger windows (T_H 9-by-9, T_L 11-by-11) have a larger count of high threshold pixels (T_H 9-by-9) and a smaller count of low threshold pixels (T_L 11-by-11) for class 5 as compared to class 6. It is interesting to note that classes 6 (Q2*cd*) and 7 (Q2*cl*), which are darker and lighter desert pavement classes of the same age, cannot be separated by the textural features (Figure 5), because of their similar topographic and drainage characteristics. However, the spectral bands accomplish the separation.

Significant improvements were also found in the separation of class 1, light bedrock, from the light-colored sands and silts of class 10 (Figure 6). Class 1 (ROCKL) and class 10 (SAND), both high reflectance classes, are inseparable in the Landsat bands, but once again are differentiated by texture (Figure 6). Thus, it appears that the inclusion of textural features improves the separation of spectrally similar but texturally dissimilar bedrock and alluvial classes.

A comparison of classification maps "spectral" and "spectral plus textural" (Plates 1 and 2) to the geologic/geomorphic sketch map and the Landsat image shows marked improvement in the "spectral plus textural" map. For example, the prominent inselberg in the north center of the image is nearly obscured by misclassified pixels in the "spectral" map, but is clearly differentiated in the "spectral plus textural" map. Likewise, the transition from rock mass to pediment along the southern margin of the image is not evident in the

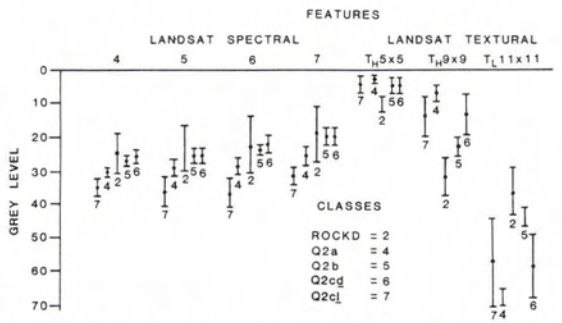

FIG. 5. Grey-level plots for classes 2, 4, 5, 6, and 7. Bars represent ±1 standard deviation.

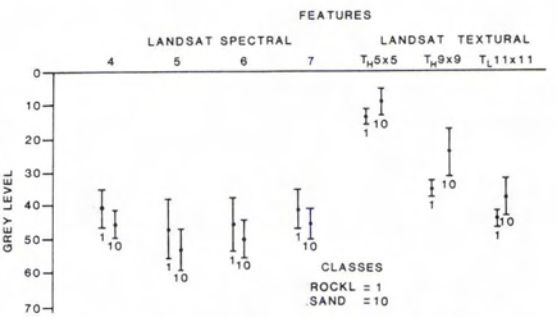

FIG. 6. Grey-level plots for classes 1 and 10. Bars represent ±1 standard deviation.

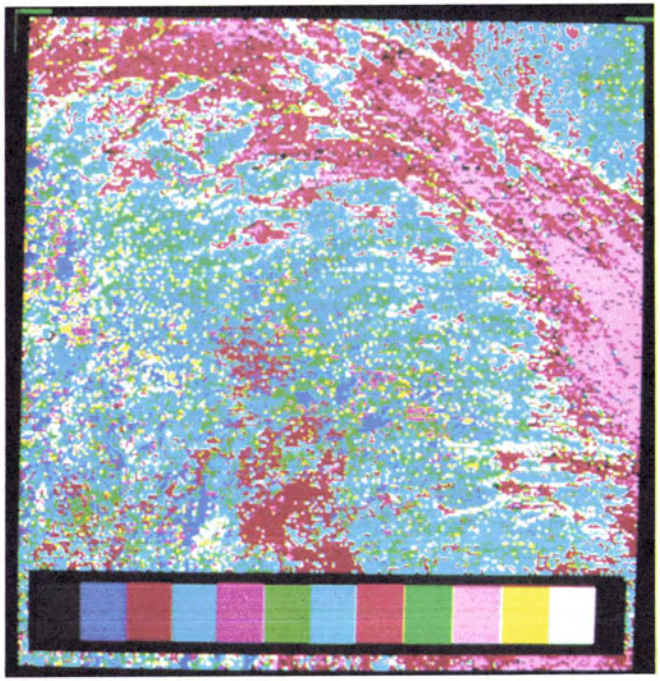

Classes	1	2	3	4	5	6	7	8	9	10	11	12
	Bedrock			Desert pavement				Eroded pavement		Fluvial deposits and vegetation		

PLATE 1. Classification Map of Landsat spectral features only.

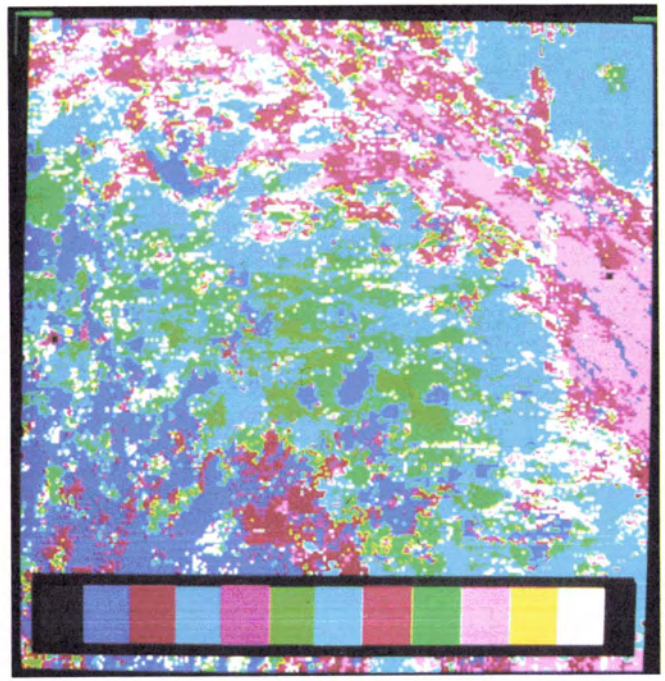

Classes	1	2	3	4	5	6	7	8	9	10	11	12
	Bedrock			Desert pavement				Eroded pavement		Fluvial deposits and vegetation		

PLATE 2. Classification Map of Landsat spectral plus textural features.

"spectral" map but is clearly delineated in the "spectral plus textural" map.

Random, single pixel misclassifications in the "spectral" map are greatly reduced in the "spectral plus textural" map. Pavement classes are clearly defined and separated in the "spectral plus textural" map whereas, in the "spectral" map, random pixel misclassifications are so frequent that class boundaries cannot be clearly defined.

Problems in classification with textural features could arise when a class is spectrally determined but contains several textures or a texture similar to other classes, and where class spatial boundaries are narrower than the window size used in the textural processing (e.g., class 12, DRP). In the latter case, thin linear, ephemeral channels appear somewhat discontinuous and blocky in the "spectral plus textural" map. The effect of this tendency is most clearly seen in the axial stream complex, which is composed (on the image) of many thin filaments corresponding to stream channels and riparian vegetation. For class 12 in this region, the "spectral" map may be more spatially accurate.

The spectral classification showed low accuracy in the mapping of the Q2a and Q2b alluvium. These classes are difficult to map because they are spatially small, are situated in the mountainous regions, and also have significant topographic relief. However, the "spectral plus textural" map separates these surfaces well. Also, the "spectral plus textural" map constrains the Q2a and Q2b classes largely to the mountainous region whereas in the "spectral" map, because of considerable spectral overlap with other pavement and bedrock classes, misclassification results in these two classes appearing throughout the pediment and basin regions.

Summary and Conclusions

Most previous remote sensing applications of textural features in computer classifications have been attempts to improve identification of urban land-use/land-cover classes (Jensen, 1979; Fasler, 1980). Little has been published on the use of textural processing in a geologic mapping application. Our experiment indicates that texture may be extremely valuable for classifying geologic/geomorphic surfaces. The overall benefit is the separation of classes that show spectral overlap but are texturally distinct. Also, random pixel misclassification, characteristic of spectral-only classifications, is reduced by the amount of textural homogeneity in a given area. Other classification improvement techniques, such as stratification, require the input of additional data, usually digital terrain data or geographical map base type data. One advantage of the use of derived textural data is that more useful information is extracted from the original data without the requirement of other additional data sets.

To permit a clear comparison of "spectral" with "spectral plus textural" classifications, we did not apply class thresholding or postclassification smoothing techniques. The use of these techniques with particular attention to the spectral versus textural qualities of individual classes is likely to further improve classification results.

The inclusion of Landsat derived textural features with spectral features can improve computer classifications of natural areas without great additional computational costs. The algorithm that was used is more sophisticated than a local variance-type textural descriptor but is comparable to it in cost. The algorithm's effectiveness when compared to more complex procedures, such as those based on Haralick's spatial dependency matrix (Haralick, 1979), is yet to be determined. It appears to be at least an order of magnitude less expensive when both are applied on a pixel-by-pixel basis.

The need for further research into the derivation, meaning, and usage of textural features is evident from this paper and studies published by other authors. Specifically, training sites need to be chosen with regard to their textural neighborhood. Because texture is by definition a neighborhood function, texture training sites also include data from the buffer zone of pixels around the actual site. Deciding what is the largest site needed to define a texture class and yet not include other neighboring textures is one problem which needs to be addressed.

The specifications of textural feature parameters such as thresholds and window sizes are usually based on empirical assumptions because few theoretical guidelines exist. Yet, the choice of histogram thresholds or window sizes may significantly affect the classification. Guidelines need to be developed for the optimum specification of these parameters, preferably based on intrinsic measurable quantities of the imagery.

Also unresolved is the problem of textural heterogeneity at complex class boundaries, which can cause misclassification if the resultant textural signatures are similar to those of other classes. This is analogous to the "mixed reflectance" pixel problem, where more than one class is represented within a pixel.

Class separability based on training site classification accuracies, *not* overall map accuracies, have been determined for the maps in this paper. The selection of appropriate test sites or other quantitative map accuracy measurements must be made in future applications. While separability between classes improved significantly, map accuracy is dependent on fully understanding which combination of field parameters controls textural and spectral signatures so that classes and classifier can be tailored (e.g., class weighting, feature weighting, etc.) to the most significant controlling

parameters. It is important to remember that, while classes are defined descriptively by the interpreter, they are defined only statistically for the computer classifier. Apparent errors in computer classification are often due solely to these differences.

Finally, application of this technique to a bedrock geologic or geologic resource problem is an obvious area of further research. The application of textural features to the Thematic Mapper bands, in conjunction with spectral ratio images, should significantly improve geologic mapping capabilities of automatically classified remotely sensed data.

Acknowledgments

This research was partially supported by Grant #14-08-0001-G-664 from the U.S. Geological Survey, EROS Program. Seed funding for this work was provided by the Geologic Society of America Grant #2528-79. Image processing was performed at the University Computer Center and the Digital Image Analysis Laboratory of the University of Arizona. Field work on the Kofa Game Range was made possible by permission of the U.S. Department of the Interior, Fish and Wildlife Service, and was supported by the Office of Arid Lands Studies and the Department of Geosciences, University of Arizona. W. B. Bull of the Geosciences Department, University of Arizona, provided valuable discussions on geomorphic interpretation. The authors wish to thank the reviewers of this paper for their comments that resulted in significant improvements in organization and clarity.

References

Bauman, A. J., 1976. Desert varnish and marine ferromanganese oxide nodules: Congeneric phenomena. *Nature*, Vol. 259, pp. 387-388.

Blake, W. P., 1904. Origin of pebble covered plains in desert regions. *Transactions of the American Institute of Mining Engineers*, Vol. 34, pp. 161-162.

Bull, W. B. In preparation. *Climatic geomorphology*. Department of Geosciences, University of Arizona, Tucson, Arizona 85721.

Carlton, S. G., and O. R. Mitchell, 1977. Image segmentation using texture and grey level. In *Proceedings IEEE Pattern Recognition and Image Processing*, pp. 387-391.

Connors, R. W., and C. A. Harlow, 1980. A theoretical Comparison of Texture algorithms. *IEEE Transactions on Pattern Analysis and Machine Intelligence*. Vol. PAMI-2, No. 3, pp. 204-222.

Cooke, R. U., 1970. Stone pavements in deserts. *Annals of the American Association of Geographers*, pp. 560-577.

Cooke, R. U., and A. Warren, 1973. *Geomorphology in deserts*. Berkeley: University of California Press, 374 p.

Dorn, R. I., 1980. A biological model of rock varnish formation. *Abstracts: Pacific Division, American Association for the Advancement of Science*. University of California, Davis, June 22-27, p. 50.

Engel, C. G., and R. F. Sharp, 1958. Chemical data on desert varnish. *Geological Society of America, Bulletin*, Vol. 69, pp. 487-518.

Fasler, F., 1980. Texture measurements from SEASAT-SAR image for urban land use interpretation. In Proceedings, American Society of Photogrammetry, Fall Technical Meeting, October 1980, pp. PS-2-B-1, PS-2-B-10.

Fenneman, H. M., 1931. *Physiography of western United States*. New York: McGraw Hill, 543 p.

Haralick, R. M., 1979. Statistical and structural approaches to texture. In *Proceedings of the IEEE*, Vol. 67, No. 5, pp. 768-804.

Haralick, R. M., K. Shanmugam, I. Dinstein, 1973. Textural features for image classification. *IEEE Transactions on Systems, Man and Cybernetics*. Vol. SMC-3, pp. 610-621.

Hooke, R. L., H. Yang, and P. W. Weiblen, 1969. Desert varnish: An electron microprobe study. *Journal of Geology*, Vol. 77, pp. 275-288.

Hsu, S. Y., 1978. Texture-tone analysis for automated land-use mapping. *Photogrammetric Engineering and Remote Sensing*, Vol. 44, No. 11, pp. 1393-1404.

———, 1979. The Mahalanobis classifier with the generalized inverse approach for automated analysis of imagery texture data. *Computer Graphics and Image Processing* 9, pp. 117-134.

Hunt, C. B., 1961. *Stratigraphy of desert varnish*. U.S. Geological Survey Professional Paper 424-B, 194 p.

Irons, J. R., and G. W. Petersen, 1981. Texture transforms of remote sensing data. *Remote Sensing of Environment*, Vol. 11, pp. 359-370.

Jensen, J. R., 1979. Spectral and textural features to classify elusive land cover at the urban fringe. *Professional Geographer*, Vol. 31, No. 4, pp. 400-409.

Jensen, J. R., and D. L. Toll, 1982. Detecting residential land-use development at the urban fringe. *Photogrammetric Engineering and Remote Sensing*, Vol. 48, No. 4, pp. 629-643.

Mitchell, O. R., C. R. Myers, and W. Boyne, 1977. A max-min measure for image texture analysis. *IEEE Transactions on Computers*, pp. 408-414.

Perry, R. S., and J. B. Adams, 1978. Desert varnish: Evidence for cyclic deposition of manganese. *Nature*, Vol. 276, pp. 489-451.

Potter, R. M., and G. R. Rossman, 1977. Desert varnish: Importance of clay minerals. *Science*, Vol. 196, pp. 1446-1448.

Scheffer, F., R. Meyer, and E. Kalk, 1963. Biologische Ursachen der Wustenlackbildung. *Zeitschrift für Geomorphologie*, Vol. 7, pp. 112-119.

Sharon, D., 1962. On the nature of hamadas in Israel. *Zeitschrift für Geomorphologie*, Vol. 6, pp. 129-147.

Shih, E. H. H., 1982. *Multispectral reflectance and image textural signatures of arid alluvial geomorphic surfaces, Castle Dome Mountains and*

Piedmont, Southwestern Arizona. Unpublished Master's Thesis, University of Arizona, 287 p.

Springer, M. E., 1958. Desert pavement and vesicular layer of some soils of the desert on the Lahonton Basin, Nevada. *Proceedings of the Soil Science Society of America,* Vol. 22, pp. 63-66.

Swain, P. H., and S. M. Davis, eds., 1978. *Remote Sensing: The Quantitative Approach.* New York: McGraw-Hill, 396 p.

Symmons, P. M., and C. F. Hemming, 1968. A note on wind-stable stonemantles in the southern Sahara. *Geography Journal,* Vol. 134, pp. 60-69.

Weszka, J., C. Dyer, and A. Rosenfeld, 1976. A comparative study of texture measures for terrain classification. *IEEE Transactions on Systems, Man and Cybernetics,* Vol. SMC-6, pp. 269-285.

Wiersma, D. J., and D. Landgrebe, 1976. The use of spatial characteristics for the improvement of multispectral classification of remotely sensed data. *Proceedings of the 1976 Symposium on Machine Processing of Remotely Sensed Data,* West Lafayette, Indiana, June 29-July 1976. IEEE, No. 76 CH1103-1 MPRSD, pp. 2A-18, 2A-26.

(Received 11 September 1981; revised and accepted 22 October 1982)

Announcement and Call for Papers
Specialist Work Shop
Pattern Recognition in Photogrammetry

Graz, Austria
27-29 September 1983

The Work Shop is being organized by Working Group III/5 of the International Society for Photogrammetry and Remote Sensing, the Austrian Working Group on Pattern Recognition, the Graz Research Center, the Technical University Graz, and the Austrian Computer Society. The main topics of the Work Shop will include

- *Reconstruction of three-dimensional object space.* Parallax detection, shape from shading, determination of sensor orientation, image transformation (rectification, etc), aircraft and satellite images, radar, medical and industrial, etc.
- *Knowledge-based image analysis and image understanding.* Knowledge models and digital maps, image-based information systems, map-guided image analysis, computer-assisted photointerpretation, use of terrain data and of image simulation, etc.
- *Data structures and conversions.* Line following, vectorization in scanned cartographic images, editing of vectorized data, effect of data structures, data compression, etc.

For further information and for submission of extended abstracts (two pages, by *30 April 1983),* please contact

Dr. F. Leberl
Techn. Univ. Graz
Wastiangasse 6
A-8010 Graz, Austria
Tele. (0316) 82531-0

Dr. M. Faintich
DMA Aerospace Center
St. Louis Air Force Station, MO 63118, USA
Tele. (314) 263-4937

Optical Science and Engineering Short Course

Doubletree Inn, Tucson, Arizona
16-27 May 1983

The purpose of the Short Course is to acquaint both the specialist and the non-specialist engineer or scientist with the latest techniques in the design and engineering of optical systems. The Course comprises 18 three-hour lectures; detailed notes will be supplied. The registration fee is $1000.

The wide range of topics that will be covered includes geometrical and physical optics, optical system layout and design, Fourier methods, polarized light, radiometry, image quality, interferometry and optical testing, lasers, thin films, photodetectors, and visible and infrared systems.

Address inquiries to

Philip N. Slater
Optical Systems & Engineering Short Courses Inc.
P.O. Box 18667
Tucson, AZ 85731
Tele. (602) 885-3798